https://ntrs.nasa.gov/search.jsp?R=19960001996 2020-06-16T06:51:37+00:00Z

NASA CR-144540

AEROSPACE REPORT NO.
ATR-92(7251)-3

NASA-CR-199540

NASA-CR-199540
19960001996

IN-46-CR
5088

(NASA-CR-199540) STORMTIME RING CURRENT AND RADIATION BELT ION TRANSPORT: SIMULATIONS AND INTERPRETATIONS (Aerospace Corp.) 17 p

N96-12004

Unclas

G3/46 0069851

Stormtime Ring Current and Radiation Belt Ion Transport: Simulations and Interpretations

1 May 1995

Prepared by

M. W. CHEN, M. SCHULZ, L. R. LYONS, and D. J. GORNEY
Space and Environment Technology Center
Technology Operations

LIBRARY COPY
MAY 31 1995
LANGLEY RESEARCH CENTER
LIBRARY NASA
HAMPTON, VIRGINIA

Prepared for

NASA Goddard Space Flight Center
Greenbelt, MD 20771

Grant No. NAGW-2126

Engineering and Technology Group

PUBLIC RELEASE IS AUTHORIZED

NF01397

THE AEROSPACE CORPORATION
El Segundo, California

TECHNOLOGY OPERATIONS

The Aerospace Corporation functions as an "architect-engineer" for national security programs, specializing in advanced military space systems. The Corporation's Technology Operations supports the effective and timely development and operation of national security systems through scientific research and the application of advanced technology. Vital to the success of the Corporation is the technical staff's wide-ranging expertise and its ability to stay abreast of new technological developments and program support issues associated with rapidly evolving space systems. Contributing capabilities are provided by these individual Technology Centers:

Electronics Technology Center: Microelectronics, VLSI reliability, failure analysis, solid-state device physics, compound semiconductors, radiation effects, infrared and CCD detector devices, Micro-Electro-Mechanical Systems (MEMS), and data storage and display technologies, lasers and electro-optics, solid state laser design, micro-optics, optical communications, and fiber optic sensors; atomic frequency standards, applied laser spectroscopy, laser chemistry, atmospheric propagation and beam control, LIDAR/LADAR remote sensing, solar cell and array testing and evaluation, battery electrochemistry, battery testing and evaluation.

Mechanics and Materials Technology Center: Evaluation and characterization of new materials: metals, alloys, ceramics, polymers and their composites, and new forms of carbon; development and analysis of thin films and deposition techniques; nondestructive evaluation, component failure analysis and reliability; fracture mechanics and stress corrosion; development and evaluation of hardened components; analysis and evaluation of materials at cryogenic and elevated temperatures; launch vehicle and reentry fluid mechanics, heat transfer and flight dynamics; chemical and electric propulsion; spacecraft structural mechanics, spacecraft survivability and vulnerability assessment; contamination, thermal and structural control; high temperature thermomechanics, gas kinetics and radiation; lubrication and surface phenomena.

Space and Environment Technology Center: Magnetospheric, auroral and cosmic ray physics, wave-particle interactions, magnetospheric plasma waves; atmospheric and ionospheric physics, density and composition of the upper atmosphere, remote sensing using atmospheric radiation; solar physics, infrared astronomy, infrared signature analysis; effects of solar activity, magnetic storms and nuclear explosions on the earth's atmosphere, ionosphere and magnetosphere; effects of electromagnetic and particulate radiations on space systems, space instrumentation; propellant chemistry, chemical dynamics, environmental chemistry, trace detection; atmospheric chemical reactions, atmospheric optics, light scattering, state-specific chemical reactions and radiative signatures of missile plumes, and sensor out-of-field-of-view rejection.

Aerospace Report No.
ATR-92(7251)-3

STORMTIME RING CURRENT AND RADIATION BELT ION TRANSPORT: SIMULATIONS AND INTERPRETATIONS

Prepared by

M. W. Chen, M. Schulz, L. R. Lyons, and D. J. Gorney
Space and Environment Technology Center
Technology Operations

1 May 1995

Engineering and Technology Group
THE AEROSPACE CORPORATION
El Segundo, CA 90245-4691

Prepared for

NASA GODDARD SPACE FLIGHT CENTER
Greenbelt, MD 20771

Grant No. NAGW-2126

PUBLIC RELEASE IS AUTHORIZED

Aerospace Report No.
ATR-92(7251)-3

STORMTIME RING CURRENT AND RADIATION BELT ION TRANSPORT: SIMULATIONS AND INTERPRETATIONS

Prepared

Margaret Chen
M. W. Chen

M. Chen for Mike Schulz
M. Schulz

L. R. Lyons
L. R. Lyons

D. J Gorney

Approved

J. B. Blake, Director
Space Particles and Fields Department

A. B. Christensen, Principal Director
Space and Environment Technology Center

Note

The material reproduced in this report originally appeared in *Space Plasmas: Coupling Between Small and Medium Scale Processes, Geophysical Monograph 86.* The ATR is published to document the work for the corporate record.

This Page Intentionally Left Blank

Stormtime Ring Current and Radiation Belt Ion Transport: Simulations and Interpretations

Margaret W. Chen, Michael Schulz[1], Larry R. Lyons, and David J. Gorney

Space and Environment Technology Center, The Aerospace Corporation, El Segundo, California

We use a dynamical guiding-center model to investigate the stormtime transport of ring current and radiation-belt ions. We trace the motion of representative ions' guiding centers in response to model substorm-associated impulses in the convection electric field for a range of ion energies. Our simple magnetospheric model allows us to compare our numerical results quantitatively with analytical descriptions of particle transport, (e.g., with the quasilinear theory of radial diffusion). We find that 10–145-keV ions gain access to $L \sim 3$, where they can form the stormtime ring current, mainly from outside the (trapping) region in which particles execute closed drift paths. Conversely, the transport of higher-energy ions ($\gtrsim$ 145 keV at $L \sim 3$) turns out to resemble radial diffusion. The quasilinear diffusion coefficient calculated for our model storm does not vary smoothly with particle energy, since our impulses occur at specific (although randomly determined) times. Despite the spectral irregularity, quasilinear theory provides a surprisingly accurate description of the transport process for $\gtrsim$ 145-keV ions, even for the case of an individual storm. For 4 different realizations of our model storm, the geometric mean discrepancies between diffusion coefficients D_{LL}^{sim} obtained from the simulations and the quasilinear diffusion coefficient D_{LL}^{ql} amount to factors of 2.3, 2.3, 1.5, and 3.0, respectively. We have found that these discrepancies between D_{LL}^{sim} and D_{LL}^{ql} can be reduced slightly by invoking drift-resonance broadening to smooth out the sharp minima and maxima in D_{LL}^{ql}. The mean of the remaining discrepancies between D_{LL}^{sim} and D_{LL}^{ql} for the 4 different storms then amount to factors of 1.9, 2.1, 1.5, and 2.7, respectively. We find even better agreement when we reduce the impulse amplitudes systematically in a given model storm (e.g., reduction of all the impulse amplitudes by half reduces the discrepancy factor by at least its square root) and also when we average our results over an ensemble of 20 model storms (agreement is within a factor of 1.2 without impulse-amplitude reduction). We use our simulation results also to map phase-space densities f in accordance with Liouville's theorem. We find that the stormtime transport of $\gtrsim$ 145-keV ions produces little change in $\bar{f}$ the drift-averaged phase-space density on any drift shell of interest. However, the stormtime transport produces a major enhancement from the pre-storm phase-space density at energies $\sim$ 30–145 keV, which are representative of the stormtime ring current.

1. INTRODUCTION

This work is an outgrowth of our continuing study of energetic charged-particle transport in the magnetosphere. The study began as an effort to understand the development of the stormtime ring current but has expanded to include the radial diffusion of radiation-belt ions. Our study entails a guiding-center simulation of particle motion in the presence of a succession of substorm-associated impulsive enhancements in the magnetospheric convection electric field. We synthesize our model storms by means of a random-number generator and apply them to a simple magnetospheric model in order to make the storm effects realistic but mathematically analyzable.

We have found, in agreement with *Lyons and Williams* [1980], that the access of $\sim$ 10–145 keV ions (having first adiabatic invariants $\mu \sim$ 1–13 MeV/G) to the region ($L \sim 3$) where they can form the stormtime ring current occurs largely as a consequence of the enhanced mean-value of the convection electric field rather than from its impulsive character. Indeed, most of the particles in this energy range that reach $L \sim 3$ in our model storm turn out to have been transported there from outside the (trapping) region in which particles execute closed drift paths. Conversely, the transport of higher-energy particles (having, for example, $\gtrsim$ 145 keV at $L \sim 3$) turns out to resemble radial diffusion across closed drift paths [cf. *Lyons and Schulz*, 1989].

By having formulated the model storm in an eas-

[1]Now at Lockheed Research Laboratory, Palo Alto, California

Space Plasmas: Coupling Between Small and Medium Scale Processes
Geophysical Monograph 86
Copyright 1995 by the American Geophysical Union

PRECEDING PAGE BLANK NOT FILMED

ily analyzed way, we are able to compare the radial diffusion coefficients obtained from our guiding-center simulation with the predictions of quasilinear theory [e g , *Fälthammar*, 1965, *Cornwall*, 1968] and various refinements thereof We find that the quasilinear diffusion coefficient calculated for any of our model storms shows a remarkably unsmooth variation with particle energy because the impulses occur at specific (although randomly determined) times Despite this, quasilinear theory provides a surprisingly accurate description of the transport process for $\gtrsim$ 145-keV ions, even for the case of an individual storm As expected, the agreement becomes even better when we reduce the impulse amplitudes systematically in a given model storm, and also when we average our results over an ensemble of model storms constructed by the same (random) method

Of course, a radial diffusion coefficient is not defined for transport from open to closed drift trajectories, such as we have found to occur for ions having 30 keV $\lesssim E \lesssim$ 145 keV For these energies, however, we find a major increase in the drift-averaged phase space density $\bar{f}$ from its pre-storm value upon mapping f in accordance with Liouville's theorem Particle energies 30–150 keV have been shown by many observational studies [e g , *Frank*, 1967, *Smith and Hoffman*, 1974, *Williams and Lyons*, 1974, *Lyons and Williams*, 1976, *Hamilton et al.*, 1988] to be representative of the stormtime ring current as a whole In contrast, we find little change in drift-averaged phase-space density as a consequence of stormtime transport for ions having $\mu \gtrsim 13$ MeV/G ($E \gtrsim 145$ keV at $R = 3$), for which the transport is diffusive

2 Field Model

The magnetic field model that we use in this study is obtained by adding a uniform southward field $\Delta\mathbf{B}$ to the geomagnetic dipole field We invoke this simple field configuration because it enables us to make direct comparisons between the simulated transport and previous analytical formulations An advantage of our model over a purely dipolar field is the presence of a quasi-magnetopause at the boundary between closed and open field lines (see Figure 1). The equation of a field line in this model is

$$[1 + 0\ 5(r/b)^3]^{-1}(r/R_E)\csc^2\theta = \text{ constant} \equiv L \quad (1)$$

where r is the geocentric distance, θ is the magnetic colatitude, R_E is the radius of the Earth, and $b = 1\ 5L^*R_E = 12\ 82\ R_E$ is the radius of the equatorial neutral line This value of b which is obtained by mapping the last closed field line (denoted L^*) to a colatitude of 20° on the Earth, corresponds to $|\Delta B| = 14\ 474$ nT and $L^* = 8\ 547$ The limit $b \to \infty$ ($L^* \to \infty$) would correspond to a purely dipolar $\mathbf{B}$ field In this study, we

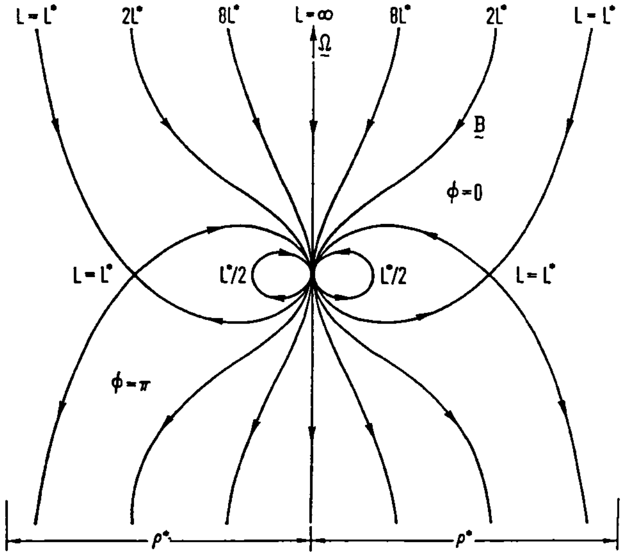

Fig 1 An illustration of the magnetospheric B-field model used in this study The model is symmetric about the $\sin\theta = 0$ axis and about the equatorial plane, which contains a circular neutral line at $r = b$ on the magnetic shell $L = L^*$, which approaches an asymptotic distance ρ^* from the tail axis at large distances $|z|$ from the equatorial plane

consider only equatorially mirroring particles in which the equatorial field intensity B_0 is given by

$$B_0 = (\mu_E/r^3) - 14\ 474 \text{ nT}, \quad (2)$$

where $\mu_E = 3\ 05 \times 10^4$ nT-R_E^3 is the geomagnetic dipole moment Further details of this field model are given by *Schulz* [1991, pp 98–110]

We assume that the total electric field $\mathbf{E} = -\nabla\Phi_E$ is derivable from the scalar potential

$$\Phi_E = -\frac{V_\Omega}{L} + \frac{V_0}{2}\left(\frac{L}{L^*}\right)^2 \sin\phi + \frac{\Delta V(t)}{2}\left(\frac{L}{L^*}\right)\sin\phi, \quad (3)$$

in which the three separate terms correspond to corotation ($V_\Omega = 90$ kV), the Volland-Stern [*Volland*, 1973, *Stern*, 1975] model of quiescent convection ($V_0 = 50$ kV), and the time-dependent enhancement $\Delta V(t)$ associated with the stormtime convection, respectively The time-varying term in the potential is assumed to vary as L [cf *Nishida*, 1966, *Brice*, 1967] rather than as L^2 because electric disturbances are expected to be less well shielded than steady-state convection by the inner magnetosphere

We model the storm-associated enhancement $\Delta V(t)$ in the cross-tail potential drop,

$$\Delta V(t) = \sum_{i=1}^{N} \Delta V_i \exp[(t_i - t)/\tau]\theta(t - t_i) \quad (4)$$

where $\theta(t)$ is the unit step function ($\equiv 1$ for $t \geq 0$, $\equiv 0$ for $t < 0$), as a superposition of almost randomly occurring impulses that rise sharply and decay exponentially with a "lifetime" $\tau = 20$ min [cf *Cornwall*, 1968] The impulses represent the constituent substorms of a storm The potential drop ΔV_i associated with any individual impulse is chosen randomly from a Gaussian distribution with a 200-kV mean and a 50-kV standard deviation We have chosen such a large mean value of ΔV_i since our intention is to model a major ($|D_{st}| \sim$ 200 nT) storm, such as those which *Lyons and Williams* [1980] analyzed Since those storms had a main phase lasting $\sim$ 3 hr, we assume that the N start times t_i in (4) are randomly distributed within a 3-hr time interval corresponding to the main phase of a storm However, we impose a 10-min "dead time" (after each impulse onset) during which no subsequent impulse can start This constraint imposes a seemingly realistic delay between consecutive impulse onsets Without such a dead-time it would be possible for the next impulse to start immediately after the previous one, and this could lead to the build-up of unrealistically large cross-tail potentials Further details of this model storm are given in [*Chen et al.*, 1992*b*]

We have constructed 100 such random storms so that on average there are 9 impulses per storm or 3 substorms/hr We have done this by generating 1800 random numbers between 0 and 100 and disqualifying about half of these through the dead-time constraint We have randomly chosen four model storms for detailed case studies Figure 2 shows the variation in cross-tail potential for these prototypical storms The mean enhancement in cross-tail potential drop for these particular storms over the time interval $t_1 < t < t_1 + 3$ hr are $\langle \Delta V(t) \rangle = 180$ kV, 178 kV, 154 kV, and 207 kV, respectively Since we choose to average over the period t_1 to $t_1 + 3$ hr, we may be excluding a significant portion of the last impulse Thus, defined in this way, the average cross-tail potential drops are typically somewhat less than 200 kV

3 Particle Dynamics

Since we simulate the guiding-center motion of nonrelativistic equatorially mirroring particles, we treat the first two adiabatic invariants ($\mu \neq 0$ and $J = 0$, respectively) as conserved quantities It follows from (2)–(4) that the guiding-center motion of an equatorially mirroring particle subject to $\mathbf{E} \times \mathbf{B}$ and gradient-B drifts is described by

$$\frac{dL}{dt} = \frac{L^2 \cos\phi}{2\mu_E {R_E}^2}\left[V_0\left(\frac{L}{L^*}\right)^2 + \Delta V(t)\left(\frac{L}{L^*}\right)\right] \quad (5)$$

and

$$\frac{d\phi}{dt} = \Omega - 3\frac{\mu\mu_E}{qB_0 r^5} - \frac{R_E}{\mu_E}\left[V_0\left(\frac{L}{L^*}\right)^2 + \frac{\Delta V(t)}{2}\left(\frac{L}{L^*}\right)\right] L \sin\phi, \quad (6)$$

where Ω is the angular velocity of the Earth, q is the charge of the particle, and ϕ is the azimuthal coordinate (local time)

We solve the ordinary differential equations (5) and (6) simultaneously by using the Bulirsh-Stoer extrapolation method with variable time-step [e g , *Press et al.*, 1986, pp 563–568] for specified initial conditions First we obtain steady-state adiabatic drift paths associated with a particular value of the first adiabatic invariant μ by setting $\Delta V(t) = 0$ in (5) and (6) Next, to study the effects of a time-dependent cross-tail potential, we start representative particles at points equally spaced in time on a steady-state drift path We do this for the purpose of properly calculating a radial diffusion coefficient and for obtaining drift-averaged phase space densities (see below) (We note that this method differs from previous simulation studies [e g , *Smith et al.*, 1979, *Lee et al.*, 1983, *Takahashi*, 1990] in which particles are injected from a nightside boundary) We then apply (4), which prescribes a storm-associated variation $\Delta V(t)$ in the cross-tail potential drop and run the simulation to determine the consequent stormtime particle transport We can run the simulation either backward in time (to determine where any representative particle must have been prior to the storm in order to reach the desired phase on its "final" drift shell) or forward in time (to follow the dispersal of initially co-drifting particles among drift shells during and after the storm)

4 Simulated Guiding-Center Trajectories

In this section we present results of simulated stormtime transport of singly charged ions having various μ values and vanishing second invariant ($J = 0$) For illustrative purposes, we present only the results that were obtained when we applied the model storm ($\langle \Delta V(t) \rangle = 180$ kV) shown in Figure 2*a* The dashed outer circle on each particle-trajectory plot shows the location of the neutral line, a circle of radius $R = 12\,82$, which marks the boundary between open and closed magnetic field lines in our magnetic-field model (cf Figure 1) Figure 3*a* illustrates steady-state trajectories of equatorially mirroring ions for $\mu = 3$ MeV/G This corresponds to an energy of 33 keV at a geocentric radial distance $r = 3\ R_E$. For this particular μ value, an x-type separatrix marks the boundary between open and closed drift trajectories We label closed drift shells in terms of the dimensionless third adiabatic invariant defined by *Roederer* [1970, p 1078] as

$$\frac{1}{L} \equiv \left|\frac{\Phi_B R_E}{2\pi\mu_E}\right| = \left[\frac{1}{2\pi}\oint\frac{d\phi}{L(\phi)}\right], \quad (7)$$

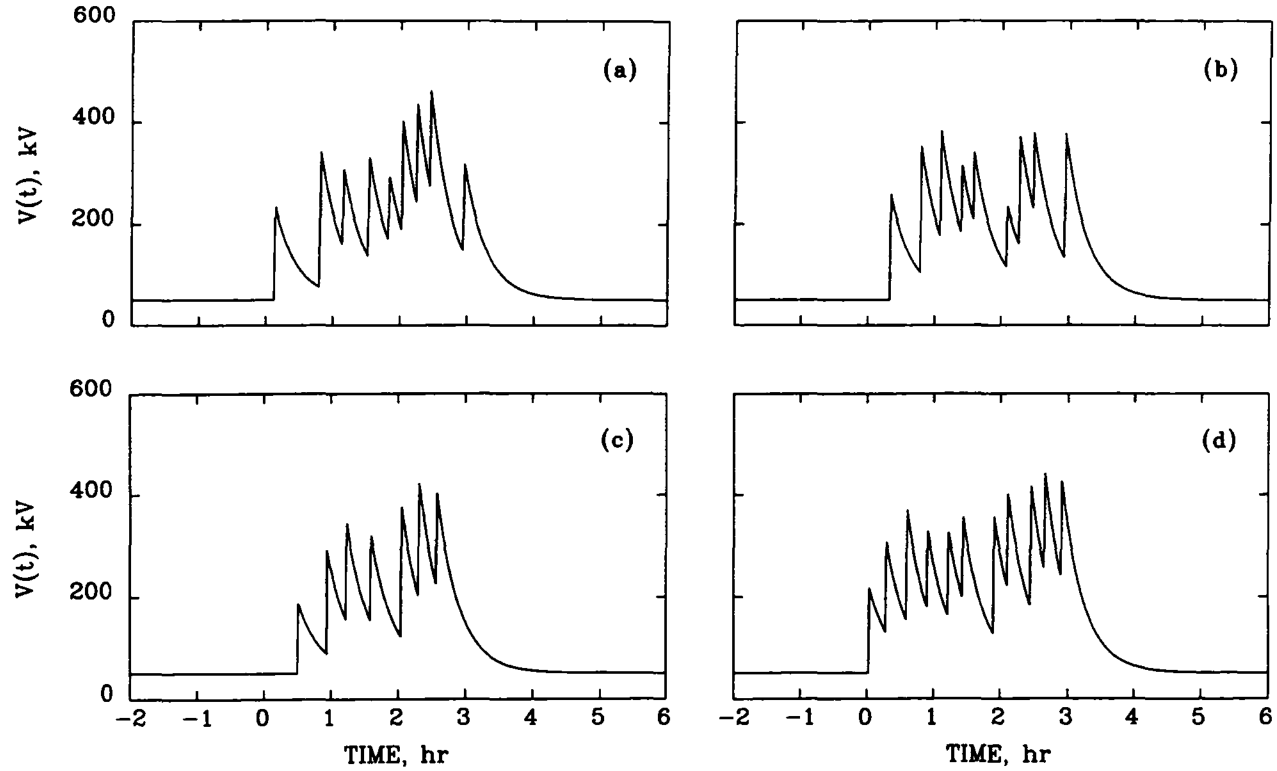

Fig 2 The cross-tail potential $V(t)$ in our model storm consists of a quiescent value V_0 (= 50 kV) and a superposition of exponentially decaying impulses (decay time τ = 20 min) These impulses represent the constituent substorms of a storm and start at times that are distributed randomly over a 3-hr time interval, except that we impose (after the start of each impulse) a 10-min "dead time" after the start of each impulse during which no subsequent impulse can start Four realizations of our model storm are shown The average enhancements $\langle \Delta V(t) \rangle$ in cross-tail potential drop over the respective 3-hr main phases are (a) 180 kV, (b) 178 kV, (c) 154 kV, and (d) 207 kV

where Φ_B is the magnetic flux enclosed by that drift shell and $L(\phi)$ denotes the field-line label at longitude ϕ on the drift shell In particular, we denote by L_1 the drift shell that separates open and closed drift paths.

We have examined the access of ions to the quiescent drift shell that intersects the dusk meridian at $R \equiv r/R_E = 3$ for a range of μ values (3 MeV/G $\lesssim \mu \lesssim$ 200 MeV/G) We select this drift shell because it is representative of where particles need to be transported in order to form the stormtime ring current We find the quiescent ionic drift period τ_3 to be 12 hr, which is longer than the assumed 3-hr main phase Starting with 12 representative ions (as indicated by the filled circles) equally spaced in time on this drift path of interest, we have run the simulation backward in time

The time-reversed trajectories shown in Figure 3*b* thus indicate where the particles must have been prior to the storm in order to have reached the final drift shell ($L \approx 3$) of interest We found that 3 of the 12 representative ions would have been transported outward from closed drift paths having smaller L values The other 9 representative ions would have been transported inward from the night side along open trajectories to populate the final closed drift path Eight of these 9 representative ions would have come from beyond the boundary of our model We have compared the time ($\sim 1-1$ 3 hr) required for these 8 representative ions to be transported inward from the neutral line to the final closed drift path of interest with the convection time [cf. *Lyons and Williams*, 1980] obtained by integrating (5) while keeping cosϕ constant in time Although *Lyons and Williams* [1980] had envisioned direct-convective access from closed drift trajectories, we have found that the direct convective access occurs mainly along open drift trajectories from the neutral line However, the access times obtained for the simulated trajectories agree reasonably well in most cases with estimates based on direct-convective access Agreement is especially good for ions transported from the nightside neutral line to the vicinity of the final drift path of interest in the quadrant centered on midnight Agreement was not as good for ions that had drifted to other local times be-

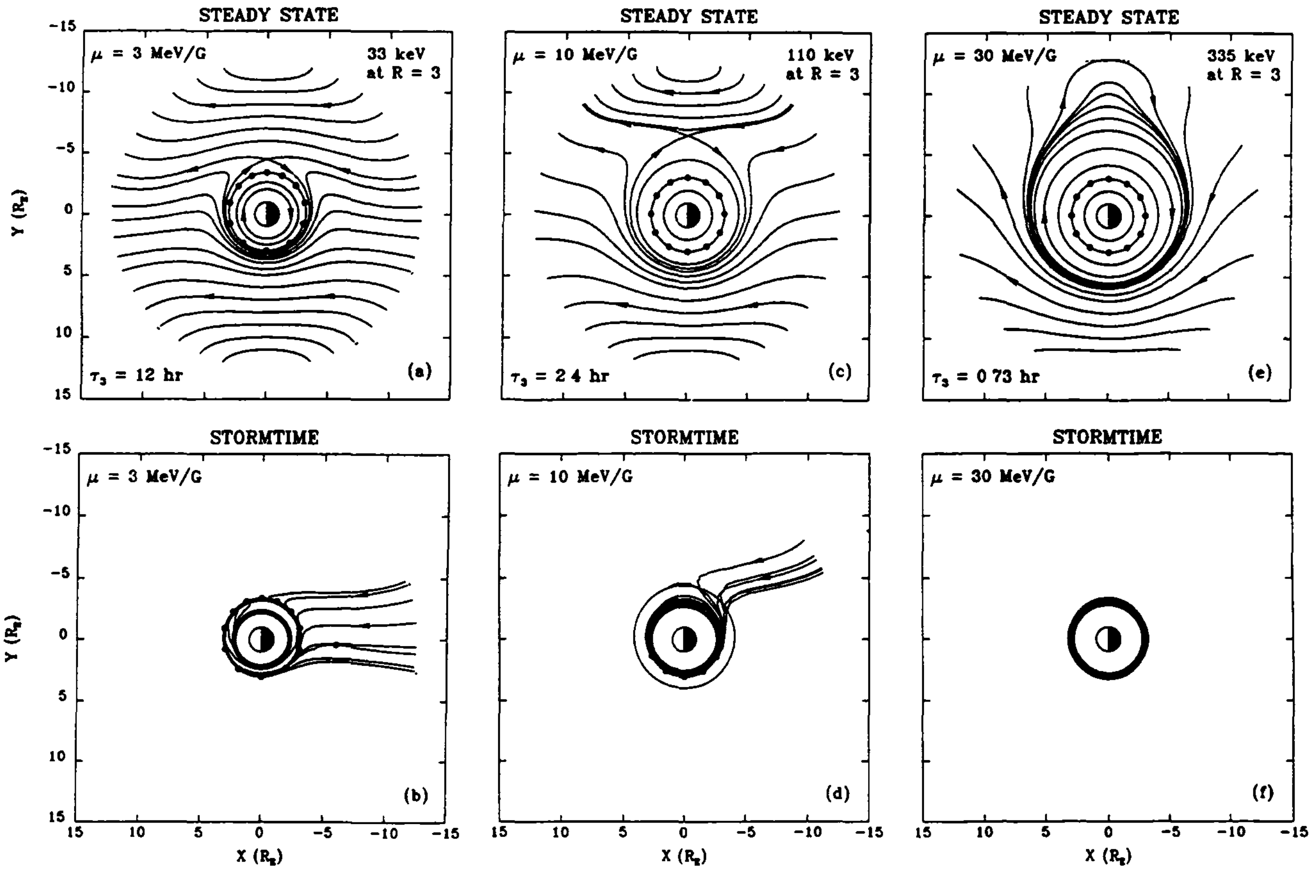

Fig 3 Quiet-time equatorial trajectories of singly charged ions having μ = 3, 10 and 30 MeV/G are plotted in the upper panels The outer dashed circle represents the neutral line at $r = b$ Ions whose drift paths cross the dusk meridian at $R = 3$ have drift periods τ_3 as noted The 12 representative ions' "final" positions on the steady-state drift path of interest are denoted by small "filled" circles Corresponding stormtime trajectories computed in our time-reversed simulation are shown in the lower panels

fore reaching the vicinity of the final drift path during the storm Reasonably good agreement was typical for lower-energy ions ($E \sim$ 30–100 keV) [*Chen et al.*, 1992*b*] and thus confirms convective access as their mode of transport

Equatorial steady-state drift paths for ions having μ = 10 MeV/G or energies of 110 keV at $R = 3$ are shown in Figure 3*c* Again, in this case, an x-type separatrix marks the boundary between open and closed drift paths The quiescent drift period (τ_3 = 2 4 hr) for these ions on a drift shell that intersects the dusk meridian at $R = 3$ is comparable to the duration of the storm's main phase

The time-reversed simulated stormtime trajectories for μ = 10 MeV/G are shown in Figure 3*d* At this μ value, only half of the representative ions have been transported to the final drift shell of interest by moving inward from the night side along open drift trajectories The other half have been transported from closed drift paths of either smaller or larger L value Their stormtime transport begins to resemble radial diffusion Thus, the mode of access of intermediate-energy ions to the stormtime ring current is transitional between convective and diffusive

Finally, we consider ions having μ = 30 MeV/G, which would correspond to energies of 335 keV at $R =$ 3. Steady-state ion drift paths are illustrated in Figure 3*e* Here the boundary between open and closed drift paths is a closed drift path tangential to the neutral line [cf *Brice and Ioannidis*, 1970, *Schulz*, 1976] Again, we consider the access of ions to the drift path that intersects the dusk meridian at $R = 3$ The quiescent drift period (τ_3 = 0 73 hr) for ions on such a drift shell is less than 1/4 of the main-phase duration

The simulated storm transports ions to the drift shell of interest from closed drift paths of either smaller or larger L value Thus, there is a spread among the initial L values of the representative particles (see Figure

3f) This transport resembles radial diffusion in this case, except that this was a time-reversed calculation We have also run a simulation forward in time, so as to follow the dispersal of ions from a common initial drift path Not surprisingly, the resulting stormtime transport generates a plot qualitatively similar to Figure 3f although the time-forward simulation applies to an implicitly different set of particles from those followed in the time-reversed simulations Transport of the type illustrated in Figure 3f was typical for ions having $\mu \gtrsim 13$ MeV/G, which corresponds to energies $\gtrsim 145$ keV at $R = 3$

Figure 3 thus illustrates a range of modes of particle access to the stormtime ring current Ions having $\mu \lesssim 5$ MeV/G ($E \lesssim 30$ keV at $R = 3$) undergo mainly direct convection from open (plasmasheet) drift paths to closed drift shells at $R \sim 3$, while ions having $\mu \gtrsim 13$ MeV/G respond to the same enhancement of the convection electric field in a manner which resembles radial diffusion among closed drift shells [cf *Lyons and Schulz*, 1989] The transition between these two idealized modes of access occurs at $\mu \sim$ 5–13 MeV/G ($E \sim$ 55–145 keV at $R = 3$) for ring-current particles whose quiescent drift periods are comparable to the duration of the model storm's main phase

5 Phase-Space Density Mapping

We have performed time-reversed ion simulations at additional μ values (1 MeV/G $\lesssim \mu \lesssim$ 100 MeV/G) for the purpose of mapping phase space distributions in accordance with Liouville's theorem to drift shells that intersect the dusk meridian at $R = 3$ This requires that we specify the distribution at the neutral line before and during the storm, and the distribution on closed trajectories before the storm At the neutral line, we maintain an exponential spectrum

$$f^* = \exp(-\mu/\mu_0) \tag{8}$$

for the phase-space density at the neutral line and set $\mu_0 = 5$ MeV/G This leads to a reasonable drop off of the boundary spectrum at high energies [cf *Williams*, 1981] We neglect losses for the distribution along open trajectories so that f^* specifies the phase space density everywhere beyond the boundary between open and closed drift trajectories (e g , see upper panels in Figure 2), which we label $L_1(\mu)$

We neglect Coulomb drag for simplicity and assume that the pre-storm transport of ions on closed trajectories is governed by an equation of the form

$$\frac{\partial \bar{f}}{\partial t} = L^2\left(\frac{\partial}{\partial L}\right)\left[\frac{D_{LL}}{L^2}\frac{\partial \bar{f}}{\partial L}\right] - \frac{\bar{f}}{\tau_q} \tag{9}$$

where $\bar{f}$ is the drift-averaged phase-space density at fixed μ and J, D_{LL} is the diffusion coefficient for transport in L, and τ_q is the ionic lifetime against charge exchange The steady-state solution to (9), in which radial diffusion balances charge exchange, can be expressed in closed form in terms of modified Bessel functions of fractional order if D_{LL} and τ_q vary as power laws in L [*Haerendel*, 1968] Thus, we seek to fit D_{LL} and τ_q accordingly

We notice, from the plot of H^+ charge exchange lifetime profiles (solid curves) reproduced from selected μ values from *Cornwall* [1972] in our Figure 4a, that τ_q tends to vary as a power law in L at the smaller L values Accordingly, we specify

$$\tau_q \approx L^{-8} 10^3 (\mu/4)^4 \text{ day}^{-1} \tag{10}$$

as a rough approximation corresponding to the dashed curves in Figure 4a This is a fairly good fit to the charge exchange lifetimes taken from *Cornwall* [1972] for $L \lesssim (2\ 5\mu)^{(2/5)}$, which covers most of the range of μ and L values of interest However, we hope to improve upon our fit of the charge exchange lifetimes in future work

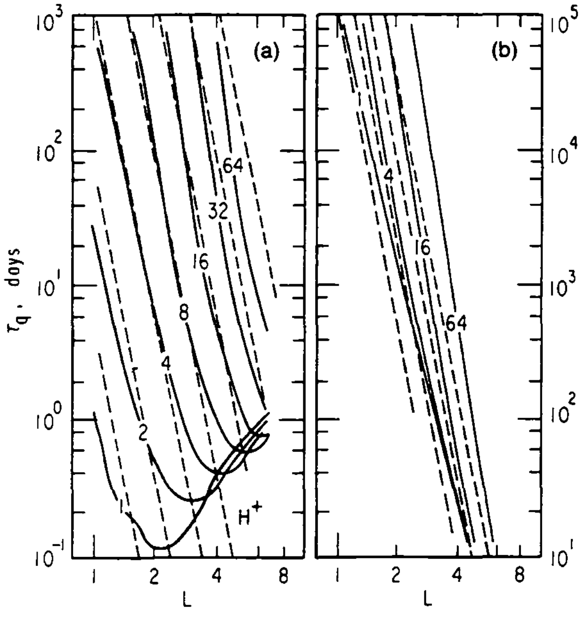

Fig 4 (a) Profiles of H^+ charge-exchange lifetimes (solid curves taken from *Cornwall* [1968]) for different values (indicated in MeV/G) of the first adiabatic invariant The formula given by (10) provides a fairly good power-law fit (L^{-8}, dashed lines) to τ_q for $L \lesssim (2\ 5\mu)^{(2/5)}$ (b) Profiles of D_{LL}^{-1}, reciprocal of the standard diffusion coefficient given by (11), for selected values of μ (indicated in MeV/G) Dashed lines represent power-law (L^{-8}) fits specified by reciprocal of (12)

Similarly, we estimate a power law fit to the diffusion coefficient The standard model [e g , *Cornwall*, 1972] leads to a diffusion coefficient of the form

$$D_{LL} \approx \frac{1\ 4 \times 10^{-5} L^{10}}{\mu^2 + L^4}\ \mathrm{day}^{-1}, \qquad (11)$$

where μ is in units of MeV/G The solid curves in Figure 4*b* are profiles of D_{LL}^{-1} for selected μ values Because the diffusion coefficient varies as L^6 for $L^2 \gg \mu$ and as L^{10} for $L^2 \ll \mu$, we have compromised on L^8 in order to obtain a single power law We thus obtain a power-law "fit"

$$D_{LL} \approx 7 \times 10^{-6} \mu^{-1} L^8\ \mathrm{day}^{-1} \qquad (12)$$

to the radial diffusion coefficient by requiring that the dashed curves in Figure 4*b* be tangent to the corresponding solid curves at $L = \mu^{1/2}$ In the future, we plan to refine our power-law model for D_{LL} (as well as for τ_q) However, for the present, our simplistic but reasonable power-law fits to the transport coefficients allow us to express the pre-storm phase-space distribution $f(\mu, L)$ by means of the equation

$$\left(\frac{L}{L_1}\right)^{5/2} \frac{f(\mu, L)}{f^*(\mu)} =$$

$$\left[\frac{I_{-5/2}(\theta) K_{-5/2}(\theta_0) - K_{-5/2}(\theta) I_{-5/2}(\theta_0)}{I_{-5/2}(\theta_1) K_{-5/2}(\theta_0) - K_{-5/2}(\theta_1) I_{-5/2}(\theta_0)}\right], \qquad (13)$$

where $\theta = L(\tau_q D_{LL})^{-1/2}$ and $\tau_q D_{LL}$ depends only on μ The inner boundary θ_0 in (13) corresponds to the drift shell that grazes the Earth's atmosphere We obtain L_0 as a very weak function of μ for this purpose by evaluating (7) for the drift shell that intersects the dusk meridian at $R = 1.1$ The outer boundary θ_1 in (13) corresponds to the separatrix $L_1(\mu)$ between closed and open drift paths (cf Figure 3, upper panels)

Using (8) and (13), we plot (see Figure 5) the pre-storm phase-space density spectrum $f(\mu, L)$ for the drift shell that intersects the dusk meridian at $R =$ 3 We distinguish between values of $f(\mu, L)$ on open (dashed curve) and closed (solid curve) drift trajectories ($\mu = 2\ 7$ MeV/G is the smallest first invariant for which the trajectories that drift through the dusk meridian at $R = 3$ are closed) Our simple model reproduces essential features similar to those found in proton phase-space distributions obtained by *Williams* [1981] from ISEE 1 data. At the higher μ values for which radial diffusion dominates charge exchange, the spectrum drops off like our exponential boundary spectrum The spectral peak (found at $\mu \sim 22$ MeV/G) had been anticipated by *Spjeldvik* [1977] and occurs mainly because the charge-exchange lifetime decreases with decreasing

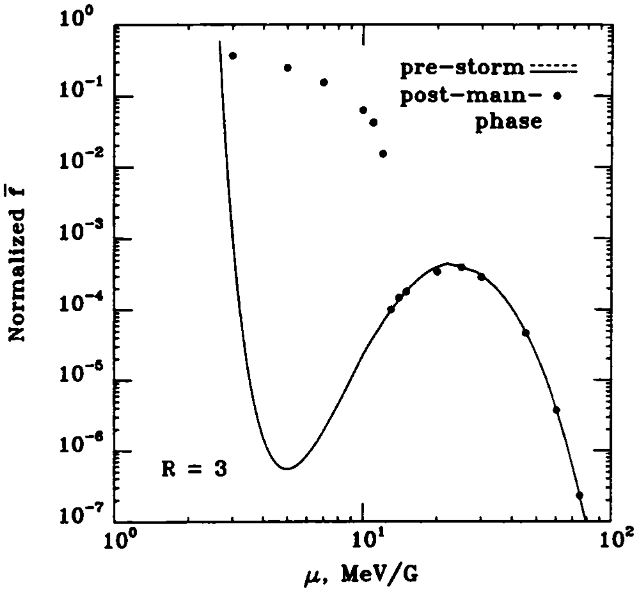

Fig 5 The pre-storm phase space density $\bar{f}$ spectrum for ions that drift through the dusk meridian at $R = 3$ is represented by the plotted curve The solid and dashed portions of the curve correspond to closed and open drift trajectories, respectively The drift-averaged phase-space density distribution (filled circles) denoted post-main-phase is obtained by averaging the mapped values of f for the 24 representative ions

μ However, since $L_1(\mu)$ also varies directly with μ for $\mu \gtrsim 1$ MeV/G, ions having small μ values do not have to diffuse as far from their boundary between closed and open drift paths in order to reach $R = 3$ (cf upper panels in Figure 3) For this reason the solution specified by (13) rises again at low μ to join the exponential boundary spectrum (dashed curve) which corresponds to ions on open drift paths

We have invoked Liouville's theorem to map the phase-space f for each representative ion from (8) and (13) For this portion of the study, we employ time-reversed tracings of 24 (cf Figure 3), rather than 12, representative ions from end-point phases equally spaced in time on a drift shell that intersects the dusk meridian at $R = 3$ By averaging the mapped f values for all the 24 representative ions we obtain a good estimate of the drift-averaged phase-space density $\bar{f}$ (filled circles in Figure 5) attained upon completion of the main phase of the model storm Our approach differs from that of *Kistler et al.* [1989] who made point-to-point mappings of phase space distributions at various local times using pre-storm spectra obtained from AMPTE data.

We find a major enhancement from the pre-storm phase-space for $\mu \sim$ 3–13 MeV/G This range corresponds to energies $\sim$ 30–150 keV, which are known to be representative of the stormtime ring current [e g , *Lyons and Williams*, 1976, *Williams*, 1981, *Kistler et al*, 1989] Moreover, these are energies for which our simulations have shown that ion transport to $L \sim 3$ occurs largely from open trajectories (e g , Figure 3*b*) In contrast, for $\mu \gtrsim 13$ MeV/G ($E \gtrsim 145$ keV at $R = 3$) we find little change in $\bar{f}(\mu, L)$ as a consequence of the transport associated with a single storm This range corresponds to particles whose transport resembles radial diffusion (e g , Figure 2*f*)

We find our preliminary results of mapping phase-space densities to be particularly satisfying since they are consistent with many observed features of ring-current phase-space distributions Thus, we are extending this study to other L-shells of interest In addition, we are refining our model for the pre-storm and boundary phase-space distributions and will report on the results in the near future

6 Diffusion and Quasi-Diffusion Coefficients

Although the higher-energy ions ($E \gtrsim$ 145 keV) do not seem to contribute much to the stormtime ring current, their diffusive transport is nevertheless interesting in the radiation-belt context Thus, we have made detailed quantitative comparisons of diffusion coefficients obtained from our simulations with predictions from the quasilinear theory of *Falthammar* [1968] For this purpose, we consider four realizations (shown in Figure 2) of our random storm model These were randomly chosen from the 100 storms that we had originally generated

For each realization of our model storm, we have computed diffusion coefficients for selected values of μ (such that 15 MeV/G $\lesssim \mu \lesssim$ 200 MeV/G) from the distribution of initial L values of the time-reversed trajectories (see Figure 3*f*) We have done this by constructing the quantity

$$D_{LL}^{sim} \equiv \left(\frac{L^4}{24T}\right)\left[\sum_{i=1}^{12}(L_i^{-1}-L_f^{-1})^2-\left[\sum_{i=1}^{12}(L_i^{-1}-L_f^{-1})\right]^2\right], \quad (14)$$

where L_i and L_f denote the drift-shell labels of the initial and final trajectories (respectively) of the 12 representative ions, and where T (= 3 hr) denotes the duration of the main phase of the model storm The quantity D_{LL}^{sim} is thus a measure of the variance among the initial third adiabatic invariants of particles situated on the final drift shell of interest We also computed diffusion coefficients D_{LL}^{sim} from time-forward simulations by interchanging the indices i and f in (14) The diffusion coefficients D_{LL}^{sim} obtained from simulations run forward and backward in time are not very different, 80% of them being within a factor of 1 6 of each other, although they pertain implicitly to different sets of particles The geometric mean discrepancies (among the 12 values of μ) between the values of D_{LL}^{sim} obtained from simulations run forward and backward in time amounted to factors of 1 3, 1 6, 1 5, and 1 8 for the four model storms in Figure 2

We compare the diffusion coefficients obtained from the simulated trajectories with the resonant-particle formulation [*Falthammar*, 1965] of radial-diffusion theory in which the diffusion coefficient is of the form

$$D_{LL}^{ql} = \frac{L^6 R_E^4}{4\mu_E^2}\hat{E}\left(\frac{\Omega_3}{2\pi}\right), \quad (15)$$

where $\hat{E}(\omega/2\pi)$ is the spectral-density of the (quasi-uniform) equatorial electric field in the inner magnetosphere and $\Omega_3/2\pi$ is the particles' quiescent drift frequency When we substitute the spectral-density function for our model storm (see *Chen et al.* [1992*b*] for derivation) into (15), we obtain the quasilinear diffusion coefficient

$$D_{LL}^{ql} = \frac{\tau^2 L^6 R_E^2}{16T\mu_E^2(L^*)^2}\sum_{i=1}^{N}\sum_{j=1}^{N}\frac{\Delta V_i \Delta V_j \cos[\Omega_3(t_j - t_i)]}{1+\Omega_3^2\tau^2} \quad (16)$$

in which correlations between the impulses lead to cross terms ($j \neq i$) By neglecting the cross terms, we could recover essentially the standard diffusion coefficient of *Cornwall* [1968], but here we retain all the cross terms in (16) for comparison with D_{LL}^{sim} as computed for individual storms

The dashed curves in Figure 6 represent the quasilinear diffusion coefficients at $L \approx 3$ for the corresponding four model storms shown in Figure 2 The respective quasilinear diffusion coefficients are not very smooth functions of μ This is because the impulse onsets (i) associated with any individual storm modeled by (4) occur at specific (although randomly determined) times t_i, which means that the corresponding spectral density $\hat{E}(\omega/2\pi)$ is not a very smooth function of frequency We plot as data points in Figure 6 the diffusion coefficients D_{LL}^{sim} obtained from simulations run forward (filled circles) and backward (open circles) in time For comparison purposes, we chose some of the μ values to correspond with the minima in D_{LL}^{ql} in case (a) Agreement of the diffusion coefficients D_{LL}^{sim} obtained from the simulations with quasilinear theory is surprisingly good despite the strong variability of D_{LL}^{ql} with μ For cases (a)–(d), we find that the geometric means of the discrepancies amount to factors of 2 3, 2 3, 1 5, and 3 0, respectively Agreement is best for case (c), in which there were only 7 substorms during the model storm (see Figure 2*c*) and consequently less variability in D_{LL}^{ql} with μ We find that quasilinear theory even accounts for the μ values (e g , $\mu = 75$ and 80 MeV/G in Figure

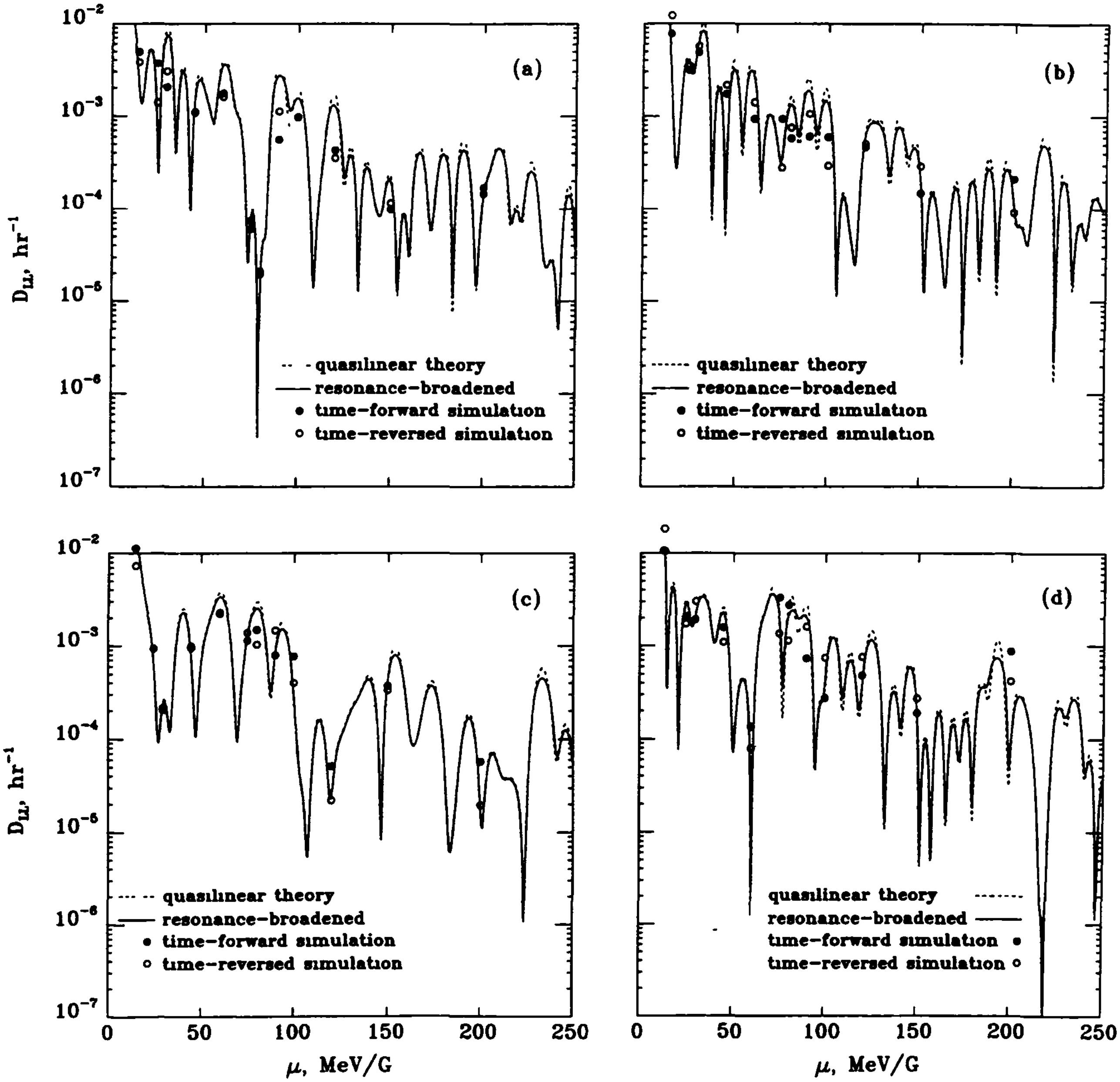

Fig 6 Plots of diffusion coefficients D_{LL}^{sim} obtained via (14) from time-reversed (open circles) and time-forward (filled circles) simulations, for comparison with the quasilinear diffusion coefficient D_{LL}^{ql} (dashed curve) given by (16) as an implicit function of μ for the four realizations of our model storm shown in Figure 2 The diffusion coefficients D_{LL}^{rb} (corrected for resonance-broadening) are represented by the solid curves

6a) for which the diffusion coefficients computed from the simulation are especially small

However, the diffusion coefficients obtained from the simulated trajectories generally do not show quite as much variability with μ as quasilinear theory predicts This is not surprising, since quasilinear theory postulates a perfectly sharp resonance at the quiescent drift frequency, whereas the simulated transport leads to an eventual spread among the quiescent drift frequencies of the representative ions for each μ A rough estimate for the anticipated spread in $\Omega_3/2\pi$ is

$$\Delta\omega/2\pi \approx (D_{LL}T/2\pi^2)^{1/2}|(\partial\Omega_3/\partial L)_\mu| \qquad (17)$$

since the mean-square spread in L accumulated during the transport is $2D_{LL}T$ [*Chen et al.*, 1992a] An estimate for the diffusion coefficient (corrected for resonance-broadening effects) is thus

$$D_{LL} \approx \frac{L^6 R_E^4}{4\mu_E^2 \Delta\omega} \int_{\Omega_3-(\Delta\omega/2)}^{\Omega_3+(\Delta\omega/2)} \hat{E}\left(\frac{\omega}{2\pi}\right) d\omega \qquad (18)$$

Since the frequency bandwidth given by (17) depends on D_{LL}, we have iterated between (18) and (17) until satisfactory convergence to the desired solution (called D_{LL}^{rb}) is achieved The results for cases (a)–(d) are plotted as solid curves in Figure 6 We find that inclusion of this nonlinear resonance-broadening effect tends to reduce the discrepancy between quasilinear theory and D_{LL}^{sim} by a smoothing out the sharp relative maxima and minima with respect to μ Corrections were typically $\sim$ 10–30% at the relative maxima but were as much as 60% at the relative minima (e g , near $\mu = 184$ MeV/G in Figure 6a). The geometric means of the remaining discrepancies between D_{LL}^{rb} and D_{LL}^{sim} amount to factors of 1 9, 2 1, 1 5, and 2 7 for cases (a)–(d), respectively To determine whether the remaining discrepancies are attributable to the neglect of nonlinear and/or quasilinear effects, we have made similar comparisons after reducing the impulse amplitudes of the enhanced cross-tail potential drop $\Delta V(t)$ in our model storms

Figures 7a and 7b show comparisons of D_{LL}^{sim} and D_{LL}^{rb} when the enhanced cross-tail potential drop ΔV for case (a) is reduced by a factors of 2 and 4, respectively When the average stormtime cross-tail potential drop decreases, the agreement between D_{LL}^{ql} and D_{LL}^{sim} improves considerably The geometric-mean discrepancy amounts to a factor of 1 4 or 1 1, respectively, when $\Delta V(t)$ is reduced by a factor of 2 or 4 The agreement is quite good despite the fact that the quasilinear diffusion coefficient does not vary smoothly with μ As the impulse amplitudes in $\Delta V(t)$ are reduced, corrections to D_{LL}^{ql} due to resonance-broadening become

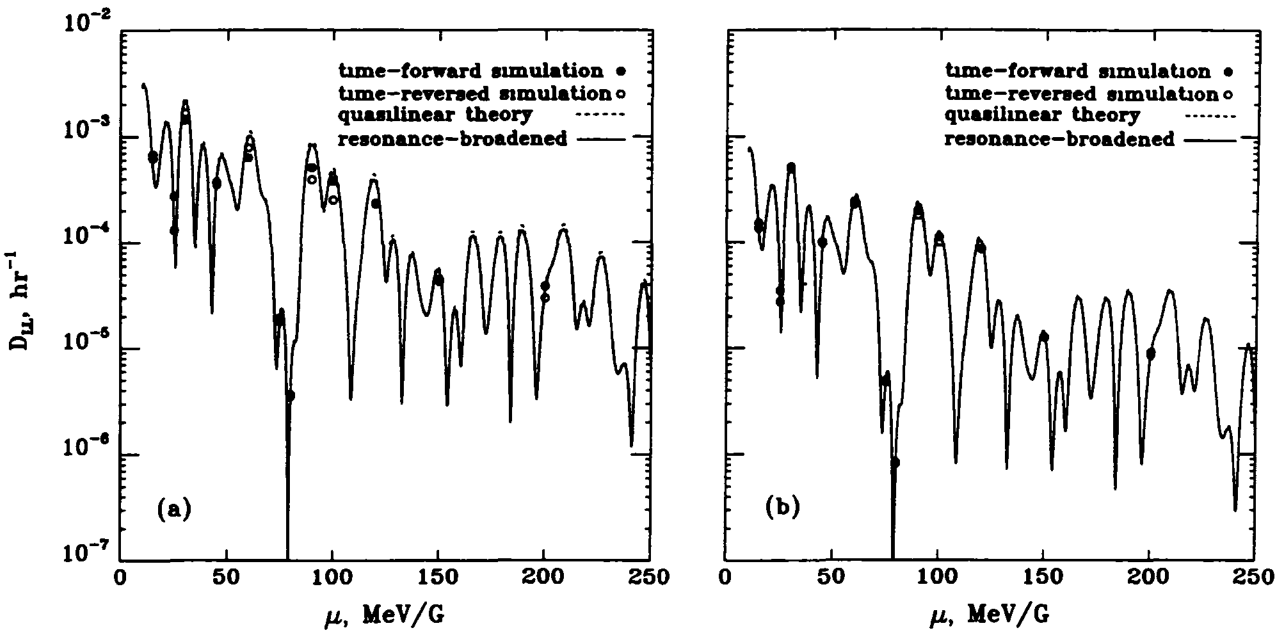

Fig 7 Plots of diffusion coefficients D_{LL}^{sim} obtained via (14) from time-reversed (open circles) and time-forward (filled circles) simulations, for comparison with the quasilinear diffusion coefficient D_{LL}^{ql} (dashed curve) given by (16) as an implicit function of μ for storms that have the same temporal structure as model storm (a) in Figure 2, but with half (left panel) and a quarter (right panel) of the impulse amplitude in $\Delta V(t)$, respectively The average enhancements $\langle\Delta V(t)\rangle$ in cross-tail potential drop over the 3-hr main phase are 90 kV and 45 kV, respectively The diffusion coefficients D_{LL}^{rb} (corrected for resonance-broadening) are represented by the solid curves

smaller, as the convergence of the solid curve (D_{LL}^{rb}) toward the dashed curve (D_{LL}^{ql}) in Figure 7*b* shows Moreover, the agreement between diffusion coefficients obtained from simulations run forward (filled circles) and backward (open circles) in time improves The geometric mean discrepancy between "time-forward" and "time-reversed" diffusion coefficients is only a factor of 1 2 when $\Delta V(t)$ is reduced by a factor of 2 and only a factor of 1 1 when $\Delta V(t)$ is reduced by a factor of 4 This improved agreement is not surprising since time reversal ($t \rightarrow -t$) leaves the quasilinear theory diffusion coefficient invariant under time reversal As $\max[\Delta V(t)] \rightarrow 0$ quasilinear theory increasingly better approximates the simulated stormtime transport, and so the values of D_{LL}^{sim} estimated from simulations run forward and backward in time become less distinct from each other We thus conclude that the remaining discrepancies between D_{LL}^{rb} and D_{LL}^{sim} are attributable to unspecified nonlinear effects of which we have not taken account

In a numerical "experiment" we found that excellent agreement between D_{LL}^{rb} and D_{LL}^{sim} could be achieved by arbitrarily increasing $\Delta\omega/2\pi$ by a factor ~ 3 from the value specified by (17). However, we can think of no physical rationale for actually postulating such a magnification of the bandwidth over which D_{LL}^{ql} should be averaged We have considered the possibility that the temporal variation of $\Delta V(t)$ in (3) might increase the spread in drift frequencies during transport (i e , for $0 < t \lesssim T$) beyond that implicit in (17), in which the factor $(\partial\Omega_3/\partial L)_\mu$ pertains to quiescent drift frequencies The guiding-center simulations presented earlier, however, show little evidence for such an effect Typically, the mean drift period of a representative ion during the main phase only slightly exceeds the quiescent drift period, as it would if the ion were drifting under the influence of a constant enhancement $\Delta V = \langle \Delta V(t) \rangle$ of the cross-tail potential drop Thus, the $\Omega_3/2\pi$ which appears in (15)–(18) should perhaps have been interpreted as the mean main-phase drift frequency rather than as the quiescent one This correction would appear to be small, corresponding to a rightward shift of the plotted curves in Figure 6 by $\Delta\mu \lesssim 1$ MeV/G However, the stormtime presence of $\langle \Delta V(t) \rangle$ does transform the quiescent drift shell of interest into a stormtime band of drift shells over which $\hat{E}(\Omega_3/2\pi)$ should presumably be averaged We will explore the ramifications of this refinement elsewhere In our simulations the transport-induced spread in quiescent drift frequencies has in some cases exceeded (17) by $\sim 40\%$, but this magnification of $\Delta\omega/2\pi$ would be too little to eliminate the remaining discrepancies ~ 1 9 between D_{LL}^{rb} and D_{LL}^{sim} in Figure 6 The very small change in the drift frequency during the storm also seems to eliminate the possibility of trapped-particle effects A preliminary test suggests that the replacement of L^6 in (15) by its transport-averaged value $\langle L^6 \rangle$ would also be a relatively unimportant nonlinear correction

7 Diffusion Averaged over Storm Ensemble

It could be argued that quasilinear theory is more appropriately applied to an ensemble of model storms than to an individual storm We have tested this hypothesis by randomly choosing 20 different storms having a 184-kV mean cross-tail potential drop from the 100 storms that we constructed We averaged the diffusion coefficients obtained from the simulations, standard quasilinear theory, and the resonance-broadened quasilinear theory over the 20 storms The results are shown in Figure 8 [*Chen et al*, 1992*b*] The ensemble-averaged quasilinear diffusion coefficient $\bar{D}_{LL}^{ql}$ (dashed curve) and its resonance-broadened counterpart $\bar{D}_{LL}^{rb}$ (solid curve) are considerably smoother than D_{LL}^{ql} and D_{LL}^{rb}, respectively, for an individual storm The ensemble-averaged diffusion coefficients $\bar{D}_{LL}^{sim}$ from the time-reversed and time-forward simulations (open circles and filled circles, respectively) typically agree much better with the theoretical diffusion coefficients in Figure 8 than does D_{LL}^{sim} with the theoretical diffusion coefficients for an individual storm in Figure 6 The mean discrepancy between $\bar{D}_{LL}^{sim}$ and $\bar{D}_{LL}^{ql}$ is only a factor of 1 2

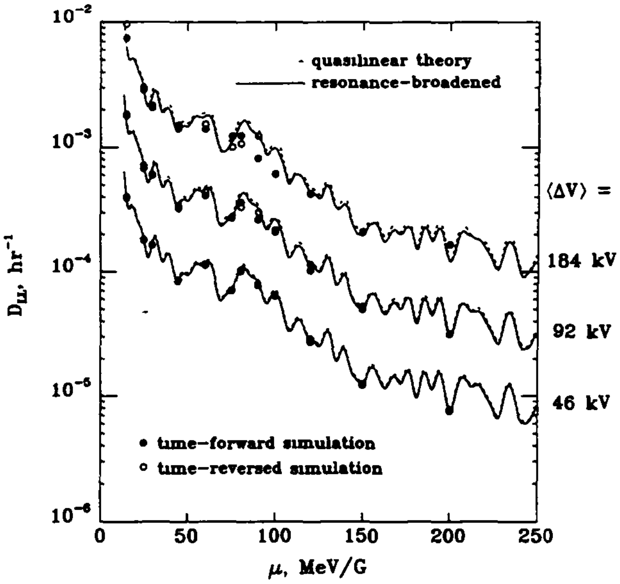

Fig 8 Ensemble-averaged diffusion coefficients $\bar{D}_{LL}^{sim}$ obtained from the time-reversed (open circles) and time-forward (filled circles) simulations, for comparison with quasilinear theory ($\bar{D}_{LL}^{ql}$ as a function of μ, dashed curve) for equivalent ensembles of 20 storms, but with impulse amplitudes halved and doubled relative to the middle family of curves and data points so as to produce the mean $\Delta V(t)$ values shown The solid curve represents the ensemble-averaged diffusion coefficients $\bar{D}_{LL}^{rb}$ corrected for resonance broadening effects

We have also halved the impulse amplitudes of ΔV in the 20 storms of our ensemble and averaged the resulting diffusion coefficients obtained over the 20 storms The results are shown via the middle family of curves and data points in Figure 8 As expected agreement between $\bar{D}_{LL}^{sim}$ and $\bar{D}_{LL}^{ql}$ is even better (geometric-mean discrepancy is a factor of 1 1 for $\langle \Delta V(t) \rangle = 92$ kV versus 1 2 for $\langle \Delta V(t) \rangle = 184$ kV) Corrections of D_{LL}^{ql} due to resonance broadening are smaller in this case

When we reduce all the impulse amplitudes in $\Delta V(t)$ by a factor of 4, we find remarkably good agreement among the ensemble-averaged diffusion coefficients obtained by the various methods For example, the geometric-mean discrepancy between D_{LL}^{sim} and D_{LL}^{ql} amounts to a factor of 1 03 and the geometric-mean discrepancy between the diffusion coefficients deduced from time-forward and time-reversed simulations amounts to a factor of only 1 02 (see lower family of curves and data points, Figure 8)

8 SUMMARY AND CONCLUSIONS

We have used a dynamical guiding-center model to investigate energetic charged-particle transport in response to storm-associated impulses in a model of the convection electric field Our simple magnetospheric model allows us to compare our numerical results with analytical descriptions of particle transport such as the quasilinear theory of radial diffusion [*Falthammar*, 1965] Thus, we have tested whether quasilinear theory can appropriately be applied to describe the charged-particle transport caused by electrostatic electric field fluctuations over time intervals as short as an individual storm Furthermore, we have begun to use our simulation results to map phase-space distributions from the quiet-time to the stormtime ring current by using Liouville's theorem A summary of our results follows

Ions having $\mu \lesssim 3$ MeV/G ($E \lesssim 110$ keV at $R = 3$) gain access to closed drift shells at $R \sim 3$ mainly by direct convection from open (plasmasheet) drift paths At $L \sim 3$ these ions have drift periods that exceed the duration of the main phase of the storm The mode of access of ions with $\mu \sim 5$–13 MeV/G ($E \sim 55$–145 keV at $R = 3$ appears to be transitional between convective and diffusive access At $L \sim 3$ these ions have drift periods that are comparable to the length of the main phase of the storm The stormtime transport of ions having $\mu \gtrsim 13$ MeV/G ($E \gtrsim 145$ keV at $R = 3$) resembles radial diffusion across closed drift shells At $L \sim 3$ these ions have drift periods that are smaller than the duration of the main phase of the storm.

The electric spectral density derived from our model storm is not very smooth, and so the quasilinear diffusion coefficient D_{LL}^{ql} does not vary smoothly with μ When we compared the diffusion coefficients D_{LL}^{sim} obtained from the simulated trajectories with the quasilinear diffusion coefficient $D_{LL}^{ql}(\mu, L)$, we nevertheless found surprisingly good agreement for 4 distinct individual model storms The aggregate geometric-mean of discrepancies between D_{LL}^{sim} and D_{LL}^{ql} for the 4 storms amounted to a factor of 2 2 even though D_{LL}^{ql} varied irregularly with μ by 4–5 orders of magnitude for each of the storms studied When we invoked nonlinear drift-resonance broadening effects, we found that the discrepancies between quasilinear theory and D_{LL}^{sim} were slightly reduced through a smoothing of the sharp relative minima and maxima in D_{LL}^{ql} The aggregate geometric mean of the remaining discrepancies between D_{LL}^{sim} and D_{LL}^{ql} for the 4 different storms amounted to a factor of 2 0 When we reduced the impulse amplitudes in the enhanced cross-tail potential drop $\Delta V(t)$ of our model storm, the agreement between D_{LL}^{ql} and D_{LL}^{sim} improved considerably For example, the geometric-mean discrepancy is a factor of 2 3, 1 4, and 1 1, respectively for a particular storm with $\langle \Delta V \rangle = 180$ kV, 90 kV, and 45 kV This convergence towards 1 0 suggests that the discrepancies between D_{LL}^{sim} and D_{LL}^{ql} are attributable to nonlinear effects When we averaged D_{LL}^{ql} and D_{LL}^{sim} obtained over an ensemble of 20 random storms, we found even better agreement between $\bar{D}_{LL}^{ql}$ and $\bar{D}_{LL}^{sim}$ (mean discrepancy amounted to a factor of 1 2 for $\langle \Delta V(t) \rangle \approx 184$ kV) When we reduced the impulse amplitudes in $\Delta V(t)$ for all the storms in the ensemble by a factor of 4, we found remarkably good agreement between these ensemble-averaged diffusion coefficients (mean discrepancy factor was 1 02)

We developed a simple model of the pre-storm (steady-state) phase-space density, obtained by balancing radial diffusion against charge exchange, which produces features qualitatively similar to those found in observations We used our time-reversed simulations to map phase space densities f from pre-storm to stormtime in accordance with Liouville's theorem The stormtime transport of ions having $\mu \gtrsim 13$ MeV/G ($E \gtrsim 145$ keV at $R = 3$), for which the transport resembles radial diffusion, seems to produce little change in drift-averaged phase space density $\bar{f}$. However, the stormtime transport of f produced a major enhancement in $\bar{f}$ from the pre-storm phase-space density at energies $\sim 30 - 145$ keV, which are representative of the stormtime ring current These are energies for which our simulations have shown that many of the ions are transported on the nightside from open trajectories to the final drift shell ($L \sim 3$) of interest

Our preliminary results on the mapping of phase space densities are particularly satisfying since they reproduce many observed features of ring-current phase-space distributions Thus, we are performing additional mappings to other L-shells of interest We plan to refine our treatment of the pre-storm and boundary phase-space distributions so as to achieve a more realistic model We also will include loss processes such as charge exchange in our simulations so that we can map phase space distributions through the recovery phase as well as through the main phase of a model geomagnetic storm

Acknowledgments The authors thank Wendall Horton for suggesting to decrease the amplitude of our electric field impulses in order to test for nonlinear effects Our work is supported by the NASA Space Physics Theory Program under grant NAGW-2126 One of the authors, Margaret W. Chen, was a National Research Council Research (NRC) Associate during this study Computing resources for this work were provided by the San Diego Supercomputer Center and by the NASA Center for Computational Sciences

REFERENCES

Brice, N M, Bulk motion of the magnetosphere, *J Geophys Res*, *72*, 5193–5211, 1967

Brice, N M, and G A Ioannidis, The magnetospheres of Jupiter and Earth, *Icarus*, *13*, 173, 1970

Chen, M W, M Schulz, L R. Lyons, and D J Gorney, Ion radial diffusion in an electrostatic impulse model for stormtime ring current formation, *Geophys Res Lett*, *19*, 621-624, 1992*a*.

Chen, M W, M Schulz, L R. Lyons, and D J Gorney, Stormtime transport of ring-current ions, re-submitted to *J Geophys Res*, August, 1992*b*.

Cornwall, J M, Diffusion processes influenced by conjugate-point wave phenomena, *Radio Sci*, *3*, 740–744, 1968

Cornwall, J M, Radial diffusion of ionized helium and protons A probe for magnetospheric dynamics, *J Geophys Res*, *77*, 1756–1770, 1972

Dungey, J W., Effects of electromagnetic perturbations on particles trapped in the radiation belts, *Space Sci Rev*, *4*, 199–222, 1965

Falthammar, C-G, Effects of time-dependent electric fields on geomagnetically trapped radiation, *J Geophys Res*, *70*, 2503-2516, 1965

Frank, L A, On the extraterrestrial ring current during geomagnetic storms, *J Geophys Res*, *72*, 3753–3768, 1967

Haerendel, G, Diffusion theory of trapped particles and the observed proton distribution, in *Earth's Particles and Fields*, edited by B M McCormac, pp 171–191, Reinhold, New York, 1968

Hamilton, D C, G Gloeckler, F M Ipavich, W Studemann, B Wilken, and G. Kremser, Ring current development during the great geomagnetic storm of February 1986, *J Geophys Res*, *93*, 14,343–14,355, 1988

Kistler, L M, F M Ipavich, D C Hamilton, G Gloeckler, B Wilken, G Kremser, and W Stüdemann, Energy spectra of the major ion species in the ring current during geomagnetic storms, *J Geophys Res*, *94*, 3579–3599, 1989

Lee, L C, G Corrick, and S-I Akasofu, On the ring current energy injection rate, *Planet Space Sci*, *31*, 901–911, 1983

Lyons, L R., and M Schulz, Access of energetic particles to storm time ring current through enhanced radial "diffusion", *J Geophys Res*, *94*, 5491–5496, 1989

Lyons, L R, and D J Williams, Storm associated variations of equatorially mirroring ring current protons, 1–800 keV, at constant first adiabatic invariant, *J Geophys Res*, *80*, 216–220, 1976

Lyons, L R., and D J Williams, A source for the geomagnetic storm main phase ring current, *J Geophys Res*, *85*, 523–530, 1980

Nishida, A, Formation of a plasmapause, or magnetospheric plasma knee by combined action of magnetospheric convection and plasma escape from the tail, *J Geophys Res*, *71*, 5669–5679, 1966

Roederer, J G., *Dynamics of Geomagnetically Trapped Radiation*, Springer, Heidelberg, 1970

Schulz, M, Effect of drift-resonance broadening on radial diffusion in the magnetosphere, *Astrophys Space Sci*, *36*, 455–458, 1975.

Schulz, M, Plasma boundaries in space in *Physics of Solar Planetary Environments*, edited by D J Williams, Vol 1, pp 491–504, Am Geophys Union, Washington, D C, 1976

Schulz, M, The magnetosphere, in *Geomagnetism*, edited by J A Jacobs, vol 4, pp 87–293, Academic Press, London, 1991

Smith, P H, and R. A Hoffman, Ring current particle distributions during the magnetic storms of December 16–18, 1971, *J Geophys Res*, *78*, 4731–4737, 1973

Smith, P H, N K Bewtra, and R A Hoffman, Motions of charged particles in the magnetosphere under the influence of a time-varying large scale convection electric field, in *Quantitative Modeling of Magnetospheric Processes*, edited by W P Olson, pp 513–535, American Geophysical Union, Washington, D. C, 1979

Spjeldvik, W N, Equilibrium structure of equatorially mirroring radiation belt protons, *J Geophys Res*, *82*, 2801–2808, 1977

Stern, D P, The motion of a proton in the equatorial magnetosphere, *J Geophys Res*, *80*, 595–599, 1975

Takahashi, S, T Iyemori, and M Takedo, A simulation of the storm-time ring current, *Planet Space Sci*, *38*, 1133–1141, 1990

Volland, H, A semiempirical model of large-scale magnetospheric electric fields, *J Geophys Res*, *78*, 171–180, 1973

Williams, D J, Phase space variations of near equatorially mirroring ring current ions, *J Geophys Res*, *86*, 189–194, 1981

Williams, D J, and L R Lyons, The proton ring current and its interaction with the plasmapause Storm recovery phase, *J Geophys Res*, *79*, 4195–4207, 1974

M W Chen, L R Lyons, and D J Gorney, The Aerospace Corporation, P O Box 92597, M2-260, Los Angeles, CA 90009

M Schulz, Lockheed Research Laboratory, Org 91-20, Bldg 255, 3241 Hanover Street, Palo Alto, CA 94304

End of Document